

## Impact of Silicon Wafer Orientation on the Performance of Metal Source/Drain MOSFET in Nanoscale Regime: a Numerical Study

Z. Ahangari<sup>\*a</sup>, M. Fathipour<sup>b</sup>

<sup>a</sup> Department of Electrical Engineering, Science and Research Branch, Islamic Azad University, Tehran, Iran

<sup>b</sup> School of Electrical and Computer Engineering University of Tehran, Tehran

### Article history:

Received 3/12/2012

Accepted 9/2/2013

Published online 1/3/2013

### Keywords:

Nanoscale Schottky

Non-equilibrium Green's

Function (NEGF) formalism

Quantum Transport

Resonant Tunneling

### \*Corresponding author:

E-mail address:

z.ahangari@gmail.com

Phone: 98 21 82084329

Fax: +98 21 88778690

### Abstract

A comprehensive study of Schottky barrier MOSFET (SBMOSFET) scaling issue is performed to determine the role of wafer orientation and structural parameters on the performance of this device within Non-equilibrium Green's Function formalism. Quantum confinement increases the effective Schottky barrier height (SBH). (100) orientation provides lower effective Schottky barrier height in comparison with (110) and (111) wafers. As the channel length of ultra thin body SBMOSFET scales down to nanoscale regime, especially for high effective SBHs, quantum confinement is created along the channel and current propagates through discrete resonance states. We have studied the possibility of resonant tunneling in SBMOSFET. Resonant tunneling for (110) and (111) orientations appear at higher gate voltages.

2013 JNS All rights reserved

## 1. Introduction

Conventional ultimately scaled MOSFET with doped source/ drain suffers from a high series resistance of ultra shallow source/ drain junctions. Schottky barrier source/ drain MOSFET (SBMOSFET) has been introduced as an alternative structure to conventional MOSFETs in nanoscale regime [1-4]. One of the solutions for enhancing the on-state current in SBMOSFET is to seek for the channel orientation with high current injection. Quantum transport and channel-

orientation dependence of p-channel SBMOSFET has been studied in [5]. Wafer orientation dependence has not been considered for n-channel SBMOSFET. The main goal of this paper is to employ the Non-equilibrium Green's function (NEGF) approach for the study of quantum transport in n-type SBMOSFET in order to investigate the influence of wafer orientation and structural parameters on the electrical characteristics of this device. As the effective SBH increases, due to quantum confinement [6] or

Fermi level pinning, the source/drain Schottky barriers and the channel form a quantum well in the channel which leads to the formation of resonance states in the transport direction [7, 8]. Resonant tunneling may be observed in SBMOSFET especially in its ultimate scaling limit.

We have considered SBMOSFET similar to a resonant tunneling diode in which multiple resonance states are modulated by the gate voltage and are contributed to the current. Impact of wafer orientation which may have a fundamental role on the effective SBH and can affect resonant tunneling is discussed extensively in this paper.

### 2. Numerical Simulation procedure

The NEGF formalism and the effective mass approach are employed to simulate quantum transport in nanoscale SBMOSFET. The longitudinal and transverse effective mass of electron on wafer orientations in which the main axes of the conduction band constant energy ellipsoids do not match with the axes of the device, must be revised. In order to apply the effective mass model on arbitrarily orientated wafers, the technique in [9] is used for calculating the effective mass. The effective mass of metallic source/drain in the transport direction is chosen the same as that of the silicon [6]. Ballistic transport is assumed in our study. The structure of the simulated double gate transistor is shown in Fig. 1a.

The 2D Hamiltonian in the double gate structure is as follows:

$$\left[-\frac{\hbar^2}{2m_x^*} - \frac{\hbar^2}{2m_z^*} + U(x, z)\right]\Psi(x, z) = E \Psi(x, z) \quad (1)$$

where  $m_x$  and  $m_z$  indicate the effective mass of electron in the transport ( $x$ ) and vertical

confinement direction( $z$ ) respectively.  $U(x, z)$  is the 2D electrostatic potential in the channel. There are two approaches for solving this 2D differential equation.

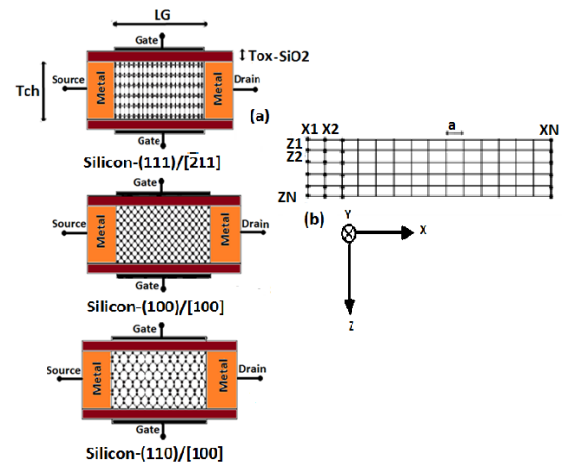


**Fig. 1.** (a) Double gate SOI MOSFET with metal source/drain simulated in this study. (b) 1D Schrodinger equation is solved in each slice in depth of the channel at each grid in the transport direction.

In real space which is computationally time consuming, the eigenvalue problem must be solved in all the individual mesh grids in the device [10]. Besides real space approach, there is another way to solve the 2D Hamiltonian in the channel of SBMOSFET with channel thickness less than 5nm; it is called the subband decomposition (mode space) method [10, 11]. In mode space approach 1D Schrodinger equation is solved in each slice in depth of the channel at each grid in the transport direction, see Fig. 1b. Hard wall boundary condition is considered in depth of the channel.

$$\left[-\frac{\hbar^2}{2m_z^*} + U(x, z)\right]\psi(x, z) = E_z(x) \psi(x, z) \quad (2)$$

$E_z(x)$  is the eigenenergy or vertical mode and  $\psi(x, z)$  is the eigenfunction in vertical direction at each  $x$  grid. Only few modes are considered

because modes (subbands) with high energies are not occupied by the carriers and do not contribute to the current. The uncoupled mode space approach treats electrons in each mode separately because no potential variation in the vertical direction is assumed. For calculating current in the transport direction, Schrodinger equation must be solved with open boundary condition. The energy of the vertical mode is added to the Hamiltonian as the potential energy in the transport direction. NEGF formalism is applied to solve the transport problem.

$$[-\frac{\hbar^2}{2m_x^*} + E_z(x)]\varphi(x, z) = E_L(x) \varphi(x, z) \quad (3)$$

$E_L(X)$  is the eigenenergy and  $\varphi(x)$  is the eigenfunction in the  $x$  direction. The retarded Greens function  $G$  is as follows:

$$G = [E_L(x)I - H - \Sigma_S - \Sigma_D] \quad (4)$$

$\Sigma$  is the self-energy caused by the coupling between the channel and the source/ drain reservoirs.  $\Sigma_S$  is the self energy from the source contact and  $\Sigma_D$  is the self energy from the drain contact. For calculating electron density, spectral function ( $A$ ) is calculated from the retarded Greens function [12, 13]:

$$A \equiv [G - G^\dagger] = [A_S] + [A_D] \quad (5)$$

Where  $A_S$  and  $A_D$  are the spectral functions due to the source/drain contacts:

$$A_S = G\Gamma_S G^\dagger \quad (6)$$

$$A_D = G\Gamma_D G^\dagger \quad (7)$$

$\Gamma$  is the imaginary part of the self energy and denotes the broadening function. The 2D electron density in the channel for mode ( $i$ ) at a longitudinal energy  $E_L(X)$  is calculated as follows:

$$N_{2Di}(x) = \left(\frac{1}{\hbar a}\right) \sqrt{\frac{2m_y^* k_B T}{\pi}} \int \frac{dE_L}{2\pi} (A_S \mathcal{F}_{\frac{-1}{2}}(E_{FS} - E_L) + (A_D \mathcal{F}_{\frac{-1}{2}}(E_{FD} - E_L))) \quad (8)$$

$$\mathcal{F}_{\frac{-1}{2}}(\epsilon) = \frac{1}{\sqrt{\pi}} \int_0^\infty \frac{t^{-\frac{1}{2}}}{1 + \exp(t - \epsilon)} dt \quad (9)$$

Where  $F$  is the Fermi Dirac integral of the order of  $\frac{-1}{2}$ .  $T$  denotes the lattice temperature and  $k_B T$  is the Boltzmann constant.  $E_{FS}$  and  $E_{FD}$  are the source and drain Fermi energies, respectively. "a" is the grid spacing along the  $x$  direction. The potential distribution in the channel is obtained from the Poisson equation. Poisson equation must be solved self consistently with the Schrodinger equation. Laplace equation is numerically solved as the initial guess for the potential. This potential is used to calculate the total electron concentration in the channel. Poisson equation uses this electron concentration to update the electrostatic potential building a self consistent loop until convergence is achieved and a certain error criteria are satisfied. The Poisson equation is as follows:

$$\left(\frac{\partial^2}{\partial x^2} + \frac{\partial^2}{\partial y^2}\right) U(x, z) = -\frac{q^2}{\epsilon} n_{3D}(x, z) \quad (10)$$

Where  $n_{3D}(x, z)$  is the total 3D electron concentration in the channel. For calculating current in SBMOSFET, the transmission probability for the energies in the transport direction,  $T(E_L)$ , with NEGF formalism must be calculated as follows:

$$T(E_L) = \text{trace}(\Gamma_S G \Gamma_D G^\dagger) \quad (11)$$

Total current for the coherent transport must be summed over all transverse modes (i) and valleys:

$$I = \frac{2q}{h} \sum_V \sum_i \int dE_L T_i(E_L) \left[ \mathcal{F}_{\frac{-1}{2}}(E_{FS} - E_L) + \mathcal{F}_{\frac{-1}{2}}(E_{FD} - E_L) \right] \quad (12)$$

### 3. Results and discussion

#### 3. 1. Electrical characteristics of SBMOSFET on arbitrarily oriented wafers

Figure 2a illustrates the calculated first lowest subband profile along the channel on arbitrarily oriented wafers. The SBH at the source/ drain channel interface is 0.25eV. The gate and drain voltages are set at 0.4V. Gate length ( $L_G$ ), the gate oxide thickness ( $T_{ox}$ ) and the channel depth ( $T_{ch}$ ) are 10nm, 1nm, and 3nm, respectively. The gate voltage is applied symmetrically to both gates. The transport direction for (100) and (110) is [100] and for (111) is [-211]. As it is depicted in Fig.2a the effective SBH at the source/ drain channel interface is increased to nearly 0.3eV for (100), 0.38eV for (110) and 0.41eV for (111) oriented wafer. They are 50meV, 130meV and 163meV higher than the defined SBH for (100), (110) and (111) wafers, respectively. The reason is that in ultra thin body fully depleted SOI MOSFET, strong confinement in depth of the channel increases the energy of the first allowed subband. As the channel thickness decreases or in the case of channel materials with lighter effective mass in the confinement direction, increase of the effective SBH is more evident. The effective mass in the vertical direction related to the first subband is

0.91 $m_0$ , 0.27 $m_0$  and 0.35 $m_0$  for (100), (110) and (111) wafers respectively. (111) and (110) provides lower effective mass in the quantization direction and the effective SBH for these orientations is higher than the effective SBH for (100) wafer.

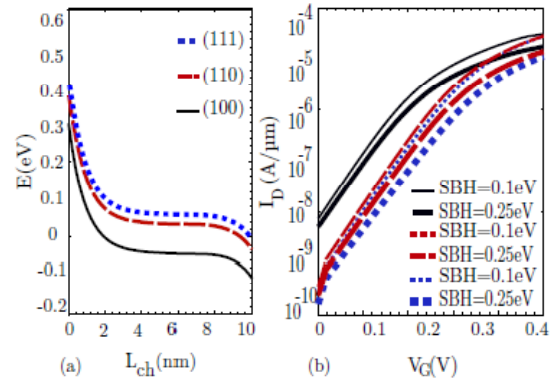


**Fig. 2.** (a) First subband profile along the channel for 3 wafer orientations;  $V_D=V_G=0.4V$  SBH=0.25eV. (b)  $I_D$ - $V_G$  characteristic of SBMOSFET on arbitrarily wafer orientations calculated for 2 different SBHs: 0.1eV and 0.25eV.

Fig. 2b reports the transfer characteristic of SBMOSFET on arbitrarily orientated wafers. Simulations are performed for two different SBHs, 0.1eV and 0.25eV. Apparently (110) and (111) wafers provides lower  $I_{off}$  in comparison with (100) due to higher effective SBH. The tunneling width increases for higher SBHs and reduces both  $I_{on}$  and  $I_{off}$  especially for (111) and (110) oriented wafers. (111) provides higher effective mass in the transport direction which reduces the tunneling probability and results in higher subthreshold slope. The transport effective mass for the lowest subband is 0.19 $m_0$ , 0.19 $m_0$  and 0.23 $m_0$  for (100), (110) and (111) orientations, respectively. Channel depth scaling increases the gate control over the channel and reduces short channel effects. As the channel thickness reduces, the effective SBH enhances and lowers  $I_{off}$ ; tunneling occurs at

higher gate voltages and the threshold voltage increases. Effective SBH versus defined SBH for  $T_{ch}=2\text{nm}$  and  $T_{ch}=5\text{nm}$  for three channel orientations is illustrated in Fig.3. For  $T_{ch}=5\text{nm}$ , the energy of the first subband shifts 16meV, 48meV and 59meV and as the channel thickness decreases to 2nm, 100meV, 300meV and 360meV is added to the energy of the first subband for (100), (110) and (111) orientations, respectively. Scaling of the channel thickness increases the effective SBH for (111) and (110) wafers more apparently than (100) wafer and it seems that (111) and (110) are not appropriate for the operation of ultrathin body n-type SBMOSFET. Wafer orientations with low effective mass in the quantization direction degrade the electrical characteristics of SBMOSFET.

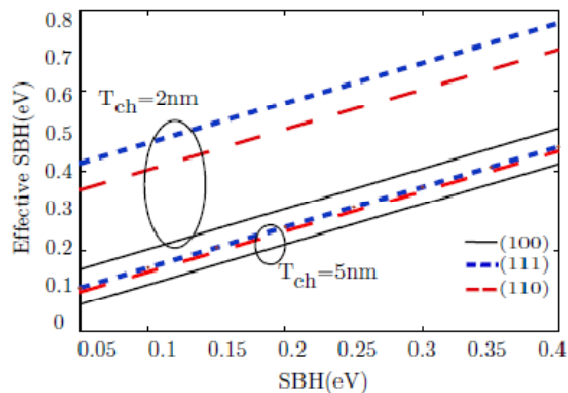


**Fig. 3.** Effective SBH versus initially defined SBH for  $T_{ch}=2\text{nm}$  and  $T_{ch}=5\text{nm}$  are calculated for 3 channel depth orientations. (110) and (111) wafers provide higher effective SBH than (100) as the channel thickness scales down to 2 nm.

### 3. 2 Resonant Tunneling Effect in SBMOSFET

In the case of low drain voltages, the high enough SBHs at the source/ drain and the channel itself form a quantum well similar to heterostructures that have been fabricated from compound semiconductors. The schottky barriers at the source/ drain pull the channel potential

towards each other and form a parabolic potential profile along the channel. In this situation, we have two quantum confinement in SBMOSFET; one in depth of the channel and the other in the transport direction. Materials with low effective mass in depth of the channel provide higher effective SBHs and quantum well like channel forms at lower SBHs. Figure 4a compares the energy of the first subband profile along the channel for two different SBHs, 0.25eV and 0.4eV at  $V_D=50\text{mV}$  and  $V_G=0.45\text{V}$  for  $T_{ch}=3\text{nm}$  as the gate scales down from 10nm to 6nm for (100) orientation. As the gate length reduces, the schottky barriers strongly affect the channel potential and besides reducing the width of the quantum well, the depth of the conduction band becomes shallow.

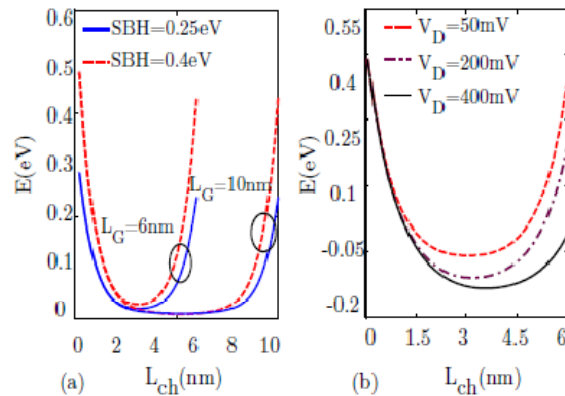


**Fig. 4.** (a) Energy of the first subband along the channel for SBH = 0.25eV and SBH = 0.4eV as the gate scales down from 10nm to 6nm at  $V_D=50\text{mV}$ ,  $V_G=0.45\text{V}$ . (b) Impact of drain voltage on the curvature of the lowest subband for SBH = 0.4eV,  $L_G=6\text{nm}$  and  $V_G = 0.45\text{V}$ . As the drain voltage increases, the curvature of the subband is smoothed out. Wafer orientation is (100).

$V_D$  plays important role in the formation of quantum well. Figure 4b illustrates impact of  $V_D$  on the profile of the lowest subband along the channel for SBH=0.4eV,  $L_G=6\text{nm}$  and  $V_G=0.45\text{V}$ . For high enough  $V_D$ , the curvature of the quantum well channel is diminished.

Local electron density of states (LDOS) along the channel for  $SBH=0.4\text{eV}$ ,  $L_G=10\text{nm}$  and  $L_G=6\text{nm}$ ,  $V_D=50\text{mV}$  and  $V_G=0.45\text{V}$  is depicted in Fig. 5. The first subband profile along the channel consists of resonant states. Each subband is like its own quantum well in E-K space. If the subband is constrained in real space in the transport direction, the resonant states within the subband will react to this spatial confinement by shifting in energy, depending on the curvature of the subband. The shape of the subband depends on the bias voltages,  $L_G$  and  $SBH$ . The energy separation between the first and the second resonant states increases from  $60\text{meV}$  to  $140\text{meV}$  as  $L_G$  scales down from  $10\text{nm}$  to  $6\text{nm}$ . It is worth mentioning that the energy separation between the resonant states varies as the gate voltage increases. Due to discrete resonant states along the channel, resonant tunneling appears in SBMOSFET due to filling of consecutive resonant states by electrons as the gate voltage is increased. In fact as long as the energy of electrons in the energy interval between  $E_{FS}$  and  $E_{FD}$  matches the energy of the localized states in the channel, resonant tunneling appears.

Resonant tunneling degrades the performance of SBMOSFET in nanoscale regime. (110) and (111) wafers provide higher effective  $SBH$  than (100) wafer. The Possibility of resonant tunneling has been elucidated for (110) and (111) wafers. Figure 6a illustrates  $I_D-V_G$  for  $SBH=0.4\text{eV}$  at  $T=77\text{K}$ ,  $V_D=50\text{mV}$  and  $L_G=6\text{nm}$  for three orientations. We have no resonant tunneling for (110) and (111) orientations. These wafers provide higher effective  $SBH$ s and lead to an increase in the minimum of the lowest subband. Hence higher gate voltage is needed for the occurrence of the first resonant tunneling. (111) orientation also has higher effective mass in the transport direction which

degrades tunneling probability as the effective  $SBH$  increases.

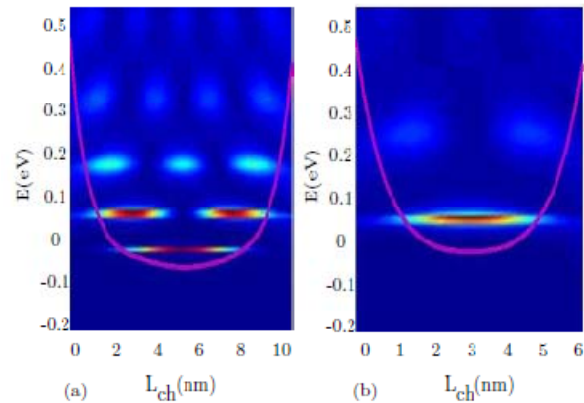


**Fig. 5.** Local electron density of states (LDOS) and first subband profile along the channel with (100) orientation at  $V_G=0.45$ ,  $V_D=50\text{mV}$ ,  $SBH=0.4\text{eV}$  for (a)  $L_G=10\text{nm}$  and (b)  $L_G=6\text{nm}$ . As  $L_G$  scales down to  $6\text{nm}$ , the energy separation between resonance states increases.

Impact of channel length on the transfer characteristic of SBMOSFET for (111) wafer orientation for  $SBH=0.4\text{eV}$ , at  $T=77\text{K}$  and  $V_D=50\text{mV}$  is presented in Fig. 6b. For  $L_G=10\text{nm}$ , multi resonance states are contributed to the current and resonant tunneling has been diminished. Current oscillation is visible in the current characteristic. For  $L_G=7\text{nm}$ , the energy separation between consecutive resonance states increases and resonant tunneling is distinguishable. As the gate length scales down to  $6\text{nm}$ , tunneling occurs only in the first resonance state and higher gate voltage is needed for tunneling through resonance states with higher energy. Resonant tunneling is visible for (100) orientation in comparison with (111) wafer as  $L_G$  scales down to nanoscale regime.



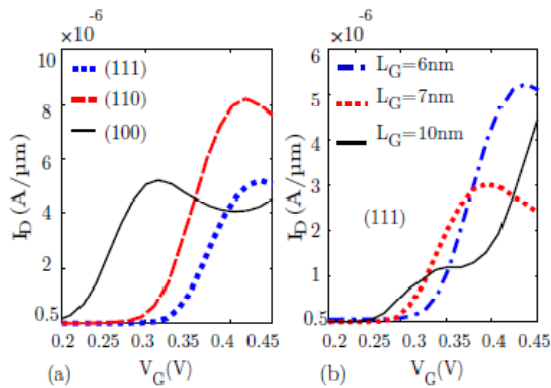


**Fig. 6.** (a) Impact of channel depth orientation on the transfer characteristic of SBMOSFET for  $V_D=50\text{mV}$ ,  $V_G=0.45\text{V}$ ,  $\text{SBH}=0.4\text{eV}$  and  $T=77\text{K}$ . Higher gate voltage is needed for the occurrence of resonant tunneling in (110) and (111) wafers. (b)  $I_D$ - $V_G$  characteristic of SBMOSFET on (111) wafer as  $L_G$  scales down to 6nm.

#### 4. Conclusion

NEGF formalism is employed to study quantum transport in SBMOSFET on arbitrarily orientated wafers to seek for the best orientation that improves the performance of this device in nanoscale regime. Tunneling is the main current mechanism in SBMOSFET and it strongly depends on the effective mass in the transport direction. (100) provides higher tunneling current in comparison with (111) and (110) wafers. Wafer orientations with low effective mass in depth of the channel, enhance the effective SBH and degrade on-state current. (111) and (110) provides higher effective SBH than (100) especially for ultra thin body devices. As SBMOSFET scales down to nanoscale regime, and especially for high effective SBHs, longitudinal quantum confinement is created along the channel and current can only propagate through discrete resonant states. Resonant tunneling appears at low temperatures and low drain voltages. Resonant tunneling occurs in (111) and (110) orientations at higher gate voltages. In order to avoid resonant tunneling in

the current characteristic of SBMOSFET in nanoscale regime, the effective SBH must be reduced. Our simulations reveal that (100) wafer improves the performance of SBMOSFET in terms of on-state current, threshold voltage and subthreshold swing.

#### Acknowledgment

The authors would like to thank Professor Mahdi Pourfath from Institute for Microelectronics, Technische Universität Wien for his useful comments.

#### References

- [1] S.Xiong, T.J. King, J.Bokor, IEEE Trans. Electron Devices, 52-8 (2005) 1859.
- [2] R.A.Vega, IEEE Trans. Electron Devices, 53-4, (2006), 866.
- [3] S. Zhu, J. Chen, M.F. Li, S.J. Lee, J. Singh, C.X. Zhu, A. Du, C.H. Tung, A. Chin, D.L. Kwong, IEEE Elec. Dev. Lett., 25-8 (2004) 565.
- [4] J.M Larson, J.P. Synder, IEEE Trans. Electron Devices, 53 (2006) 1048.
- [5] M. Shin, Appl. Phys. Lett., 97 (2010), 092108.
- [6] J. Guo, M. Lundstrom, IEEE Trans. Electron Devices, 49-11(2002) 1897.
- [7] S. Toriyama, N. Sano, J. Comput. Electron. 7 (2008) 471.
- [8] S. Toriyama, Jpn. J. Appl. Phys., 49 (2010), 104204.
- [9] A. Rahman, M. S. Lundstrom, and A. W. Ghosh, J. Appl. Phys. 97 (2005) 053702.
- [10] R. Venugopal, Z. Ren, S. Datta, and M. S. Lundstrom, D. Jovanovic, J. Appl. Phys. 92 (2002), 3730.
- [11] Z. Ren, R. Venugopal, S. Goasguen, S. Datta, IEEE Trans. Electron Devices, 50 (2003), 1914.
- [12] S. Datta, Superlattices Microstruct, 28 (2000), 253.
- [13] S. Datta, Quantum transport: atom to transistor, Cambridge, University Press, 2005.